Bažant, Z.P., and Ožbolt, J. (1990). "Nonlocal mi- croplane model: Tensile and compression fractures and triaxial damage." in *Computer-Aided Analysis and Design of Concrete Structures* (Proc., Second Int. Conf., SCI-C, Zell am See, Austria, April 4-6, 1990), ed. N. Bicanic and H. Mang, Pineridge Press, Swansea, U.K., 809–829.

COMPUTER AIDED ANALYSIS AND DESIGN OF CONCRETE STRUCTURES

Edited by:

N. BIĆANIĆ
University of Wales, Swansea, U.K.

H. MANG
Technical University, Vienna, Austria

Proceedings of SCI-C 1990, Second International Conference held in Zell am See, Austria 4th-6th April, 1990

PINERIDGE PRESS

Swansea, U.K.

NONLOCAL MICROPLANE MODEL: TENSILE AND COMPRESSION FRACTURES AND TRIAXIAL DAMAGE

Zdeněk P. Bažant[1] and Joško Ožbolt[2]

Center for Advanced Cement-Based Materials
Northwestern University
Evanston, Illinois 60208, USA

SUMMARY

After a review of current status of nonlinear triaxial models, the lecture presents a new generalized microplane model for concrete and demonstrates in finite element implementation by analysis of tensile and compression fracture specimens. A previous microplane model which was demonstrated to describe well the nonlinear triaxial response of concrete in compression and shear serves as a point of departure. To prevent spurious mesh sensitivity due to strain softening, the recently proposed concept of nonlocal damage is adopted and combined with the microplane model. The idea of exponential algorithm initially proposed for creep is adapted to the present model to obtain a very efficient step by step numerical algorithm. It is demonstrated by analysis of geometrically similar specimens of different sizes that the nominal stress at maximum load in tensile fracture specimens approximately follows the size effect law which was previously extensively verified by experiments on concrete. For compression fractures, however, analysis of specimens of different sizes reveals no significant size effect. The failure in compression is in the form of either shear band or axial splitting. The axial splitting is driven by inelastic volume dilatancy due to the deviatoric stresses at the fracture front region. The present nonlocal microplane model appears to be ready for use in finite element analysis of tensile and compression fractures as well as general nonlinear triaxial behavior.

[1]Professor of Civil Engineering
[2]Visiting Scholar on leave from University of Zagreb; presently Research Engineer at Stuttgart University

INTRODUCTION

Failure of concrete structures is characterized by progressive development of distributed damage, which presents four difficult modeling problems: (1) A realistic material model for the strain softening regime needs to be developed. (2) An effective method of analyzing strain-localization instabilities must be formulated. (3) Material properties which limit localization, e.g. the characteristic length of a nonlocal continuum, need to be determined. (4) Numerical algorithms that avoid spurious mesh sensitivity as well as mesh bias, inherent to strain softening and crack band propagation, need to be set up.

The present lecture, which summarizes two recent reports at Northwestern University (Bažant and Ozbolt, 1989 a,b), will briefly outline the microplane model as one effective approach to strain softening, analyze tensile as well as compression fracture from the view point of localization of damage, and indicate some effective numerical approaches. The exposition will be preceeded by a broader review of nonlinear triaxial models for concrete with strain softening.

CURRENT STATUS OF NONLINEAR TRIAXIAL MODELS

At present one may discern three basic types of material models for strain-softening damage:

(1) Continuum models, which need to be endowed with a nonlocal character in order to capture strain softening damage and the inherent size effects.

(2) Random particle models, in which the microstructure is imagined to consist of randomly aranged rigid aggregate pieces with elastic-softening interactions among them (Zubelewicz and Bažant, 1987; Bažant, Tabbara, Kazemi and Pijaudier-Cabot, 1989; Bazant and Tabbara, 1990).

(3) Micro-finite element models, in which the matrix as well as the aggregate pieces in concrete are subdivided into many finite elements, whose inelastic behavior and cracking as well as interface bond failures are taken into account (Roelfstra and Wittmann, 1987).

The last two approaches might eventually prove most realistic but they are still extremely demanding for computer time, especially in three dimensions, and are at present feassible only for structural parts, not entire structures. Nevertheless, these are rather promising approaches since they automatically exhibit: (a) the experimentally observed nonlocal properties, such as localization limited to a band of a certain minimum thickness; (b) the correct size effect on nominal strength of the structure, which is transitional between plasticity (no size effect) and the linear elastic fracture mechanics (the strongest possible size effect) (Bažant and Tabbara, 1990); and (c) the experimentally observed effect of structure size on the energy dissipation during failure and the mean post-peak slope of the load-deflection curve (Bažant and

Tabbara, 1990). For the analysis of concrete structures, however, the continuum approach is available at present. Even in the future it will not loose its importance since it alone provides understanding and insight. Among the continuum models, one can distinguish two basic types:

(I) The classical tensorial phenomenologic models, which describe the material directly on the macro level and use semi-intuitive arguments to properly formulate the constitutive relations in terms of tensorial invariants of stress or strain.

(II) The so-called microplane models, in which the material is characterized by a relation between the stress and strain components on planes of various orientations, characterizing the damage planes or weak planes in the microstructure, such as the contact layers between aggregate pieces in concrete.

The microplane models were initiated by an epoch-making paper of G.I.Taylor (1938), who suggested the principle for the modeling of plasticity of polycrystaline metals. In that approach, developed in detail by Batorf and Budianski (1949) and others, the plastic slips were calculated independently on various crystalographic planes based on the resolved shear stress component, and were then superimposed to obtain the plastic microstrain. Later this approach was extended, under the name multilaminate model, to the modeling of non-softening plastic response of soils or rocks (Zienkiewicz and Pande, 1977; Pande and Xiong, 1982). Recently (Bažant, 1984; Bazant and Oh, 1983, 1985; Bažant and Gambarova, 1984; Bazant and Prat, 1988), this approach was extended to include strain softening of concrete, and was renamed more generally as the "microplane model", in recognition of the fact that the approach is not limited to plastic slip but can equally well describe cracking and strain softening damage. The general term "microplane" was coined (Bažant, 1984) to replace the term "slip planes". In these studies it was also shown that, in order to prevent instability due to strain softening, the microplanes must be constrained kinematically rather than statically, in which case the use of the principle of virtual work must replace the direct superposition of the plastic strains as used in the slip theory.

A basic requirement for a continuum model for a brittle heterogeneous material such as concrete is that it must correctly display the consequences of heterogeneity of the microstructure. A continuum constitutive model lumps the average response of a certain characteristic volume of the material (Fig. 1). In essence, one may discern two types of interactions among the particles or damage sites in the microstructure, which must be somehow manifested in the continuum model: (1) Interaction at *distance* among various sizes (e.g., between A and B, Fig. 1); and (2) interaction *among various orientations* (see angle α in Fig. 1).

The interactions at distance control the localization of damage. They are ignored in the classical, local continuum models but are reflected in nonlocal models (Bažant and

effects are hidden in $\Delta\sigma''_{ij}$, which is a tensor of fewer components than C_{ijkm}, and is therefore more efficient in computations. When the tangential stiffness tensor C^t_{ijkm} is needed, e.g. for the analysis of stability and path bifurcations, its values are obtained by calculating the stress responses to prescribe unit states of incremental strains.

It has been shown that, by virtue of the split of the normal microplane strain into its volumetric and deviatoric parts, the microplane model can exhibit any value of the Poisson's ratio between -1 and 0.5. Furthermore, the ratio C_V/C_D can be chosen arbitraily, so as to yield the best data fit. An optimum value of this ratio is usually between 0.25 and 1.0.

In fitting of nonlinear triaxial test data for concrete, the Young's modulus and Poisson's ratio are known in advance, and the parameters for the hydrostatic response curves can also be determined by simple curve fitting separately. Several other parameters can be fixed once for all, and there remain only four material parameters which need to be varied to fit test data and are capable of providing excellent fit (Bazant and Prat, 1988). Thus, the fitting of triaxial test data with the microplane model proved to be far easier than with the previous phenomenologic tensorial models such as endochronic or plastic fracturing, in which a much larger number of parameters needed to be varied.

Due to the kinematic constraint, the microplane stresses cannot be exactly equal to the resolved components of the macrostresses. The micro-macro equivalence of stresses can be enforced only approximately, which has been done by means of the principle of virtual work. This provided an incremental macroscopic stress-strain relation of the form:

$$\Delta\sigma_{ij}=C_{ijkm}\Delta\varepsilon_{km}-\Delta\sigma''_{ij} \tag{5}$$

in which

$$C_{ijkm}=\frac{3}{2}\pi\int_S\Big[(\hat{C}_D-\hat{C}_T)n_in_jn_kn_m+\frac{1}{3}(\hat{C}_V-\hat{C}_D)n_in_j\delta_{km}+ \\ +\frac{1}{4}\hat{C}_T(n_in_k\delta_{jm}+n_in_m\delta_{jk}+n_in_k\delta_{im}+n_jn_m\delta_{ik})\Big]dS \tag{6}$$

$$\Delta\sigma''_{ij}=\frac{3}{2}\pi\int_S\Big[n_in_j(\Delta\sigma''_V+\Delta\sigma''_D)+ \\ +\frac{1}{2}(n_i\delta_{rj}+n_j\delta_{ri}-2\,n_in_jn_r)\,\Delta\sigma''_{Tr}\Big]\,dS \tag{7}$$

where n_i are direction cosines of the unit normal to the microplane and δ_{ij} is the Kronecker delta. C_{ijkm} is the macroscopic incremental material stiffness tensor, and $\Delta\sigma''_{ij}$ are the associated macroscopic inelastic stress increments. The integration extends over surface S of a unit hemisphere. The integration over the unit hemisphere in Eq. 6 and 7 can be carried out very efficiently by one of the classical Gaussian-type integration formulas given by Stroud (1971) or some new superior ones (Bažant and Oh, 1986). Efficiency is here very important, since the integration over a unit hemisphere must be carried out a great number of times - in every load step, in every iteration of the step, and in every integration point of every finite element. The lowest number of numerical integration points on the unit hemisphere which gives practically sufficient accuracy is 21 (in three dimensions; in two dimensional or axisymmetric problems this number can be reduced).

EXPONENTIAL ALGORITHM FOR LOAD STEP CALCULATIONS

In every iteration of r-th load or time step , we can use the known macrostrains $\varepsilon_{ij(r)}$ and their known increments $\Delta\varepsilon_{ij(r)}$ to calculate the strains and strain increments on each microplane based on the kinematic constraint. Then we can use the known values of $\varepsilon_N=\varepsilon_V+\varepsilon_D$, ε_{Ti}, $\Delta\varepsilon_N=\Delta\varepsilon_V+\Delta\varepsilon_D$, and $\Delta\varepsilon_{Ti}$, to calculate the stresses on each microplane by solving the differential Eq. 3. Each of these equations could be solved by using a central difference approximation. However, such an approximation often appears unstable when the stress-strain relation has a negative slope (strain softening). Even if the computations remain stable, a large error is usually accumulated, with the result that the stress is not reduced exactly to zero at very large strains.

These drawbacks can be eliminated by the so-called exponential algorithm, initially developed for aging creep of concrete (Bažant, 1971) and later extended to creep with strain softening and applied by Bažant and Chern (1985). We will now adopt the exponential algorithm to the microplane model.

The basic idea of the exponential algorithm is that the integration formula is the exact solution of the differential equation obtained for the loading step under the assumption that the material properties, the loads and the prescribed rates are constant in time. To develop the formula of exponential algorithm for our case, we proceed similarly to Bažant and Chern (1985), introducing the Maxwell's spring-dashpot model for stress relaxation. The advantage is that the stress relaxation equation always ultimately yields a zero stress value if the load step is very large. For each microplane and for both normal and tangential directions, it is possible to write a relation which formally looks like the equation for the Maxwell model. Since the relations for ε_V, ε_D, and ε_T are the same, we now drop subscripts V, D and T, and from $\dot{\sigma}=C\,\dot{\varepsilon}$ we have $\dot{\sigma}=C\,\dot{\varepsilon}+\dot{C}\,\varepsilon$, i.e.

$$\dot{\sigma}+\frac{\sigma}{E}=C_a\,\dot{\varepsilon} \tag{8}$$

where the superior dots denote time derivatives, $E = -C_a/\dot{C}$, $\dot{C} = (dC/d\varepsilon)\,\dot{\varepsilon}$, $\dot{\varepsilon} = \Delta\varepsilon/\Delta t$ and $C_a = (C_r + C_{r+1})/2$ for time step number r. In every time step $\Delta t_r = t_{r+1} - t_r$, E can be approximated as a constant, and then the exact solution of Eq. 8 is of the form

$$\sigma(t) = A\, e^{-(t-t_r)/E} + C_a\, E\, \dot{\varepsilon} \tag{9}$$

where A is an integration constant. From the initial condition $\sigma = \sigma_r$ at $t = t_r$, it follows that

$$\sigma(t) = \sigma_r\, e^{-(t-t_r)/E} + (1 - e^{-(t-t_r)/E})\, C_a\, E\, \Delta\varepsilon \tag{10}$$

For the end of the time step, $t = t_{r+1} = t_r + \Delta t$, we get

$$\sigma_{r+1} = \sigma_r + \Delta\sigma = \sigma_r\, e^{-\Delta z} + (1 - e^{-\Delta z})\, C_a\, \frac{\Delta\varepsilon}{\Delta z} \tag{11}$$

in which $\Delta z = \Delta t / E = -\Delta C / C_a$. Eq.11 can be rewritten in the form of a pseudo-elastic stress-strain relation on the level of each microplane stress component

$$\Delta\sigma = D\,\Delta\varepsilon - \Delta\sigma'' \tag{12}$$

where $D = C_a\,(1 - e^{-\Delta z})\,/\,\Delta z$, $\Delta\sigma'' = D\,\Delta\varepsilon''$ and $\Delta\varepsilon'' = (1 - e^{-\Delta z})\,\sigma_r\,/\,D$; $D\,\Delta\varepsilon = \Delta\sigma_{el}$, $\Delta\sigma_{el}$ and $\Delta\sigma''$ are the elastic and inelastic stress increments.

This algorithm, as well as the similar previous ones, is called exponential because its formula involves an exponential function. Attaching subscripts V, D and T, the foregoing formulas are used to determine the stress increments on each microplane and in both normal and tangential directions. The stress increment on the macro-level is then determined using numerical integration over the unit hemisphere (with 21 integration point), as already described.

NONLOCAL GENERALIZATION

According to the nonlocal concept, already mentioned, the stress at a point depends not only on a strain at the same point but also on the strain field from a certain neighborhood of the point (Kröner 1986, Eringen and Edelen 1972, Krumhansl 1968, Levin 1971). For strain softening behavior, this concept was introduced in Bažant, Belytschko and Chang (1984). However, the early form, called imbricate continuum (Bažant, 1984), proved to be computationally to cumbersome, and a more effective form, in which all variables that are associated with strain softening are nonlocal and all other variables, particularly the elastic strain, are local, was introduced (Pijaudier-Cabot and Bažant, 1987; Bažant and Pijaudier-Cabot, 1988). An important advantage of this formulation, called nonlocal damage or nonlocal continuum with local strain, is

that the differential equations of equilibrium as well as the boundary conditions are of the same form as in the local continuum theory, and that there exist no zero-energy periodic modes of instability.

Since strain softening is in the present microplane model controlled by the damage variables ω_V, ω_D and ω_T, these variables must be calculated on the basis of the resolved microplane components of the nonlocal rather than local microstrain tensor, ε_{ij}. However, when unloading or reloading takes place, the calculation must be based on the resolved components of the actual (local) macrostrain tensor. The nonlocal microstrain, which must be evaluated at each integration point of each finite element in each loading step, is obtained as

$$\bar{\varepsilon}_{ij}(\underset{\sim}{x}) = \frac{1}{V_r(\underset{\sim}{x})} \int_V \alpha(\underset{\sim}{s}-\underset{\sim}{x})\, \varepsilon_{ij}(\underset{\sim}{s})\, d\underset{\sim}{x} = \int_V \alpha'(\underset{\sim}{s},\underset{\sim}{x})\, \varepsilon_{ij}(\underset{\sim}{s})\, d\underset{\sim}{x} \tag{13}$$

in which $\underset{\sim}{x}$ and $\underset{\sim}{s}$ are the coordinates vectors, $\alpha(\underset{\sim}{x})$ is a given empirical weighting function, V is the volume of the structure, and

$$V_r(\underset{\sim}{x}) = \int_V \alpha(\underset{\sim}{s}-\underset{\sim}{x})\, dV(\underset{\sim}{s}) \;, \quad \alpha'(\underset{\sim}{s},\underset{\sim}{x}) = \frac{\alpha(\underset{\sim}{s}-\underset{\sim}{x})}{V_r(\underset{\sim}{x})}. \tag{14}$$

In numerical integration, the spatial averaging integral is approximated by a finite sum over all the integration points of all finite elements of the structure (this is simpler to program than taking a sum over only some points, but of course the weight coefficients for many remote points are zero). The values of α' are generated in advance and are stored as a matrix. $V_r(\underset{\sim}{x})$ has approximately the same meaning as the representative volume in the statistical theory of heterogeneous materials (Kröner, 1968). When the averaging volume protrudes outside the boundary of the body, the points outside the body are simply imagined to be chopped of and weights of the remaining points are then scaled up from α to α', so that the sum of all the weights in the averaging integral would remain the same. It may be noted that the scaling from α to α' causes the matrix of α' to become nonsymmetric, and thus introduce nonsymmetry into the tangential stiffness matrix. But this has not be found to cause any computational problems. The weighting function has been considered in the present computation in the form:

$$\alpha(\underset{\sim}{x}) = \left[1-(\rho/\rho_1)^2\right]^2 \quad \text{for} \quad \rho < \rho_1; \quad \alpha = 0 \quad \text{for} \quad \rho \geq \rho_1 \tag{15}$$

which gives an equation of a bell shape; $\rho = r/kl$, $\rho_{12} = R/kl$, and for 1D: $r^2 = x^2$, $k = 15/16 = 0.9375$; for 2D: $r^2 = (x^2 + y^2)$, $k = \sqrt{3/4} = 0.9086$; for 3D: $r^2 = (x^2 + y^2 + z^2) = 105/192$) $= 0.8178$. These values of k were determined from the condition that the volume under function $\alpha(\underset{\sim}{x})$ should be equal to the volume under the function $\bar{\alpha}(\underset{\sim}{x})$ that is uniform over the representative volume of length of diameter l (the characteristic length of nonlocal continuum).

Nonsymmetry is also introduced into the tangential

stiffness matrix when adjacent points that are loading or unloading appear simultaneously in the same spatial averaging integral. Again, this asymmetry has not been found to course numerical difficulties. By using in the iterations a stiffness matrix based on the initial elastic stiffness, any need for solving systems of equations with a nonsymmetric matrix is of course avoided. Thus, the symmetry breaking nonlocal response is incorporated into the inelastic nodal forces.

A preceding paper (Bažant and Ožbolt, 1989 a) describes an effective numerical iterative algorithm for the loading steps, similar to that used previously for the local microplane model.

NUMERICAL STUDIES OF TENSILE FRACTURE AND SIZE EFFECT

Finite element calculations have been made using four-node isoparametric finite elements, with one integration point in example 1 and four integration points in example 2. The nonlocal microplane model as already described has been used.

As the first example, the concrete specimen shown in Fig. 2, loaded in tension, has been analyzed. Only one of the specimen was modelled, assuming symmetric response. The strain localization was initiated by assuming some finite elements to be weaker, having the initial elastic modulus smaller by 5% than the remaining elements (the shaded elements in Fig. 2).

The microplane model parameters defined in Bazant and Prat, 1988, had the values: a = 0.005, b = 0.035, b = 1.0, q = 1.85, e_1 = 0.00006, e_2 = 0.0004, e_3 = 0.0004, m =1.2, n = 1.1, k = 1.1, E_0 = 30000 N/mm^2, and ν = 0.18. The nonlocal characteristic length was assumed to be l = 150 mm. To demonstrate the mesh sensitivity in the case of strain softening, two different meshes were analyzed (Fig. 2), one with 21 and the second with 84 finite elements. Fig. 3a, obtained with the local microplane model, reveals, as expected, strong mesh sensitivity. However, the results for the nonlocal microplane model shown in Fig. 3b exhibit no spurious mesh sensitivity.

As the second example, we consider tree-point-bend fracture specimens of three different sizes, in the ratio 1:2:4, and with geometrically similar shapes (Fig. 4). Exactly this type of specimen was tested at Northwestern University (Bažant an Pfeiffer, 1987) using concrete with maximum aggregate size d_a = 12.7 mm. The depth of the smallest specimen was d = 76.2 mm. For computations, the characteristic length was assumed to be $l = 3d_a$.

The microplane model parameters defined in the previous paper (Bažant and Prat, 1988), have the same values as in the first example except for some small adjustments made to fit better the test results for the smallest test specimen (a = 0.005, b = 0.035, p = 1.0, q = 1.85, e_1 = 0.000075, e_2 = 0.0012, e_3 = 0.0012, n = 0.5, m = 1.2, k = 1.2, E_0 = 35000 N/mm^2 and ν = 0.18.). The results of calculations as well as previous experiments are presented in terms of the nominal stress at

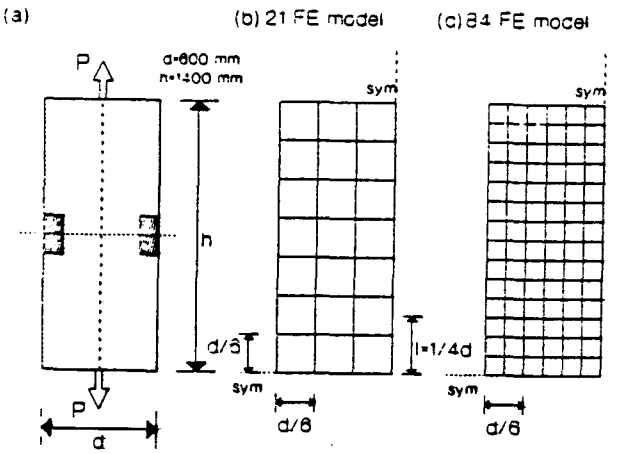

Fig. 2 Specimen loaded in tension and two different finite element meshes

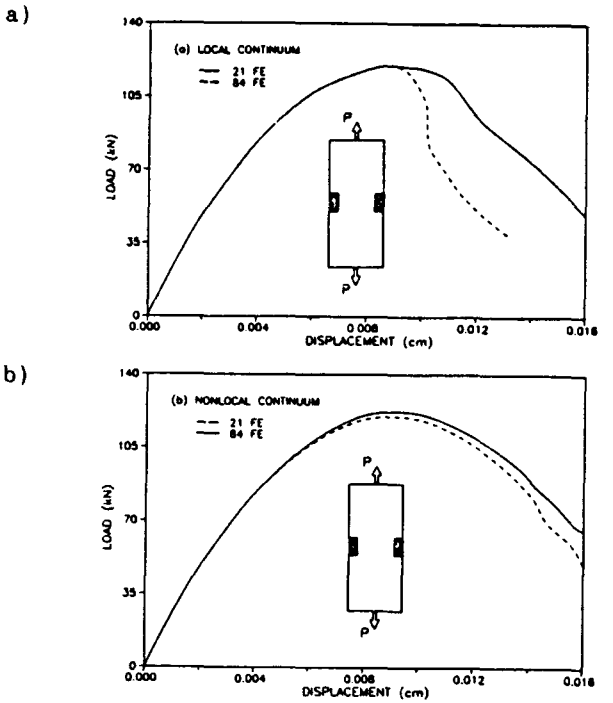

Fig. 3 Load-displacement curves for two different finite element meshes

failure, $\sigma_N = P/bd$ where b= specimen thickness (38.1 mm) and d = specimen depth; see Fig. 5a,b. The solid and dashed curves represent the optimum fit of the test results obtained with the present model and optimum fits obtained by the size effect law (Bazant, 1984):

$$\sigma_N = B\, f'_t \left[1 + (d/d_0) \right]^{-1/2} \qquad (16)$$

in which f'_t = tensile strength and B and d_0 = empirical parameters. The optimum values of B and d_0 were obtained by linear regression. From Fig. 5a,b it can be concluded that the agreement between the test results and the present calculations is quite good. The most important point is that the transitional size effect, described by the size effect law, is correctly represented by the present nonlocal form of the microplane model.

Fig. 6 shows the contour of the fracture process zone at the peak load state, as obtained for small, mediuma and large specimens. The size of this zone is found to be approximalely equal to the characteristic length, and increase slightly as the specimen size increases.

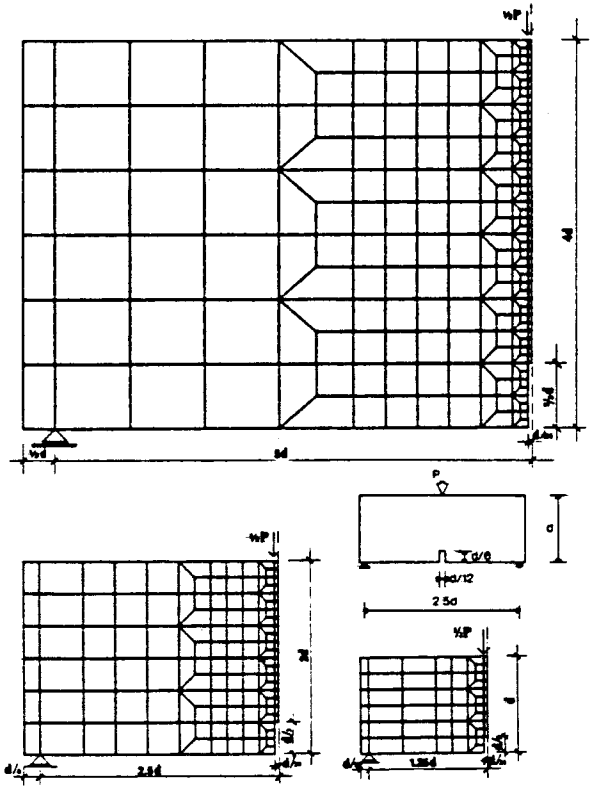

Fig. 4 Finite element meshes used for tree-point-bend specimens

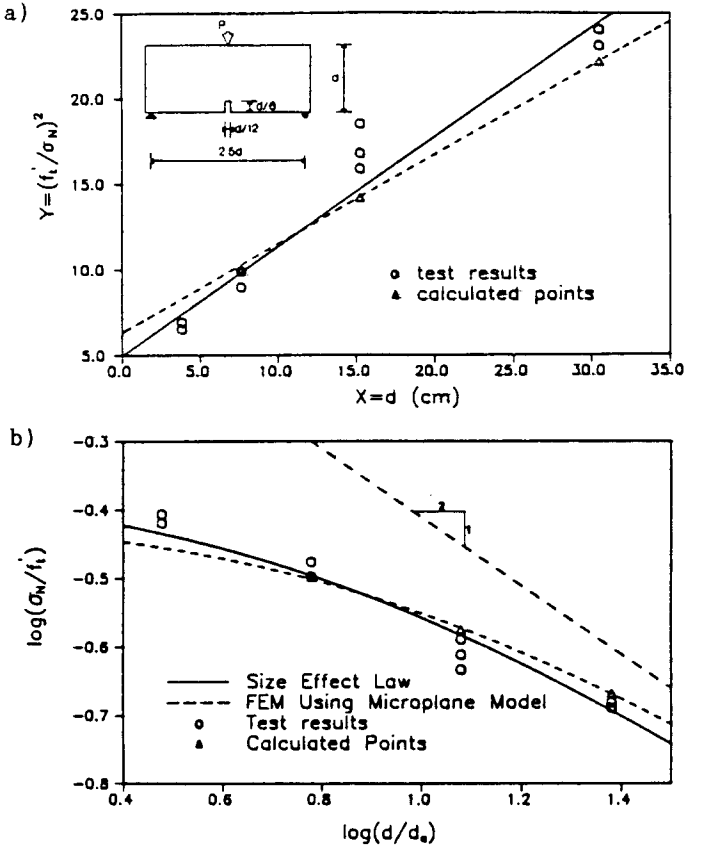

Fig. 5 Size effect

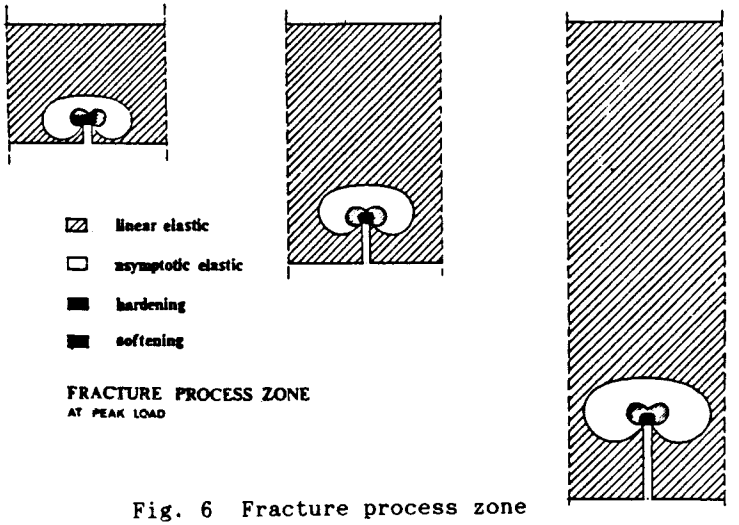

Fig. 6 Fracture process zone

NUMERICAL MODELING OF COMPRESSION SPLITTING FRACTURE

The mathematical modeling of compression fracture is a difficult problem with a long history. Brittle heterogeneous materials exhibiting progressive damage, such as concrete as well as rocks and ceramics, fail in compression either by inclined shear bands or by axial splitting. The latter failure type dominates especially in prismatic specimens in which the strain distribution just before failure appears to be macroscopically and microscopically almost uniform (this is achieved when the platens are well lubricated).

The difficulty in modeling compression splitting fracture stems principally from the fact that introduction of an axial line crack into a uniform stress field of uniaxial compression causes no change in the stress state, and thus no release of stored energy which would drive the propagation of the axial splitting fracture. Therefore, there must exist some mechanisms that brake the uniformity of the uniaxial compression stress field, or the fracture cannot be the line crack, or both.

One hypothesis for the development of a nonuniform stress field was threedimensional buckling (Bazant and Cedolin, 1990); However, that hypothesis was shown to provide reasonable results only for highly anisotropic materials, or for cases of strong stress-induced anisotropy. Probably threedimensional buckling can play only a secondary role in the axial splitting of concrete.

Another uniformity breaking mechanism can be caused by the existence of a cracking band of a finite width at the fracture front. In particular, a logical assumption seems to be (Bazant, 1988) that high deviatoric stresses in the cracking band (i.e. in the fracture process zone) produce volume dilatancy, which in turn produces transverse tensile stresses in front of the fracture process zone and thus drives the axial splitting fracture.

As is well known from the studies of nonlinear triaxial behavior, realistic prediction of volume dilatancy due to deviatoric stresses requires sophisticated triaxial constitutive model covering the strain softening. Such a model is provided by the present microplane model, for which a good description of the nonlinear triaxial behavior including volume dilatancy and post-peak response has previously been demonstrated.

We consider a uniaxially compressed rectangular concrete specimen of size 300 × 540 mm (Fig. 7). The specimen may be imagined to represent the cross section of a wall which is in a plane stress state.

The material parameters (as defined by previous study by Bazant and Prat, 1988) are: a = 0.005, b = 0.043, p = 0.75, q = 2.00, e_1 = 0.00006, e_2 = 0.0015, e_3 = 0.0015, m =1.0, n = 1.0, k = 1.0, E_0= 23500 N/mm^2, and ν = 0.18. The finite element mesh is shown also in Fig. 7. Using the aforementioned material parameters of the microplane model, calculations yield uniaxial compression strength 17.6 MPa and tensile strength 1.72 MPa.

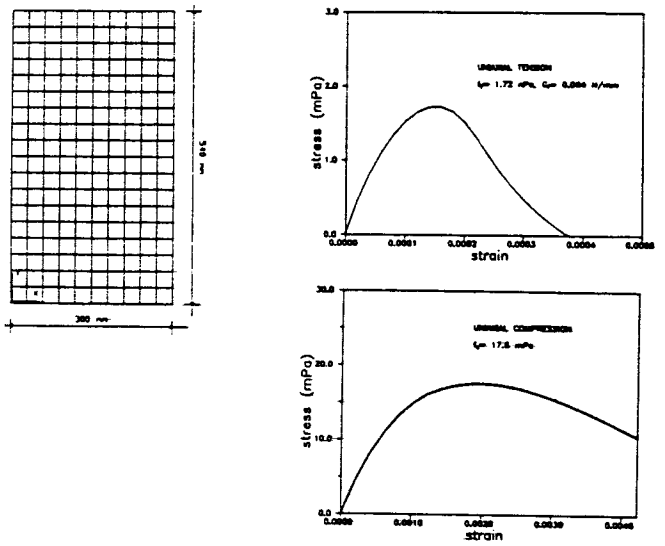

Fig. 7 Finite element mesh used in splitting compression analysis and material properties

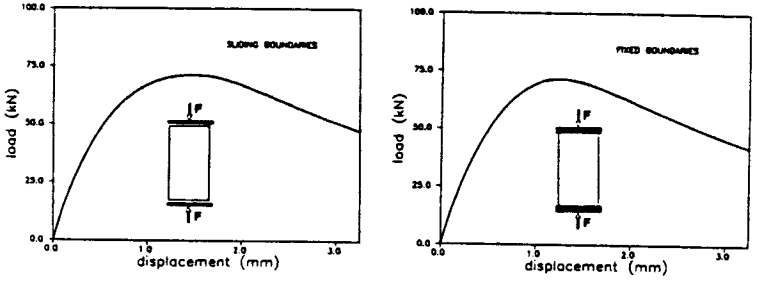

Fig. 8 Load-displacement curves

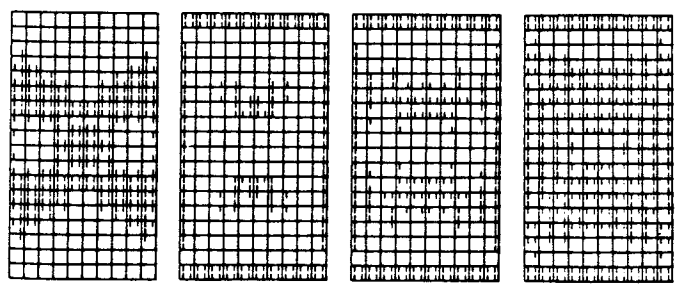

Fig. 9 Cracking zone at a different load stages (sliding boundaries)

The maximum aggregate size is d_a = 30 mm, and the characteristic length is $l = 3d_a$.

The compression specimens are analyzed for both perfectly sliding top and bottom boundaries (no friction), and fixed boundaries. The loading is introduced as enforced uniform axial displacement increments in each loading step. Since the compression splitting failure must be the result of propagation of the softening damage band in the direction of compression, there must be some small initial inhomogeneity which starts the band. Therefore we assume that in the center of the specimen there is a weak zone; see the shaded element in Fig. 7. The elastic modulus in the weaker zone is assumed to be 5% less than in the rest of the specimen. Isoparametric four-node quadrilaterals are again used in the calculations, with four integration points. All the elements are identical and their size is equal to 1/3 of the characteristic length.

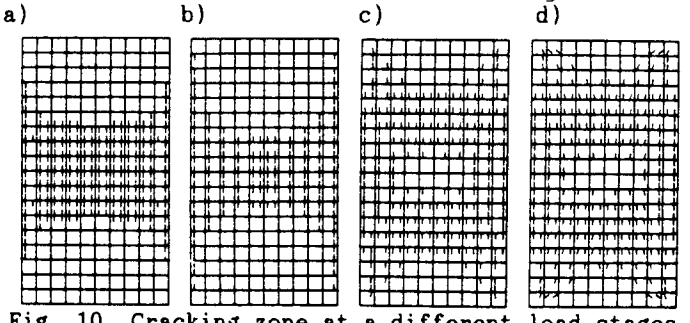

Fig. 10 Cracking zone at a different load stages (fixed boundaries)

Fig. 8 shows the calculated load-displacement curves for both types of boundary conditions. The maximum load for both cases is about the same. The displacement at the peak load is slightly larger for the case with perfectly sliding boundaries (Fig. 8a), while the softening post-peak curve for the case with fixed boundaries is steeper (Fig. 8b). Fig. 9 and 10 show the crack development at different load levels for both types of boundary conditions. At each integration point at which the maximum principal stress is positive (tension), a straight line segment is plotted in the direction perpendicular to the maximum principal stress. Fig. 9a and 10a indicate the crack direction at the start of the analysis, Fig. 9a and 10b in the hardening range, Fig. 9c and 10c at the peak-load state, and Fig. 9d and 10d in the post-peak softening range at the end of the calculations.

Fig. 9 (perfectly sliding boundaries) clearly indicates the tendency toward formation of vertical (splitting) cracks. At the start of loading, a crack initiates from the weaker zone and subsequently, due to volumetric dilatation which is caused (according to the microplane model) by deviatoric strains, the crack band propagates in the vertical direction toward the loaded boundaries. At the same time the crack at the center of the specimen starts to close. At the peak load (Fig. 9c), the

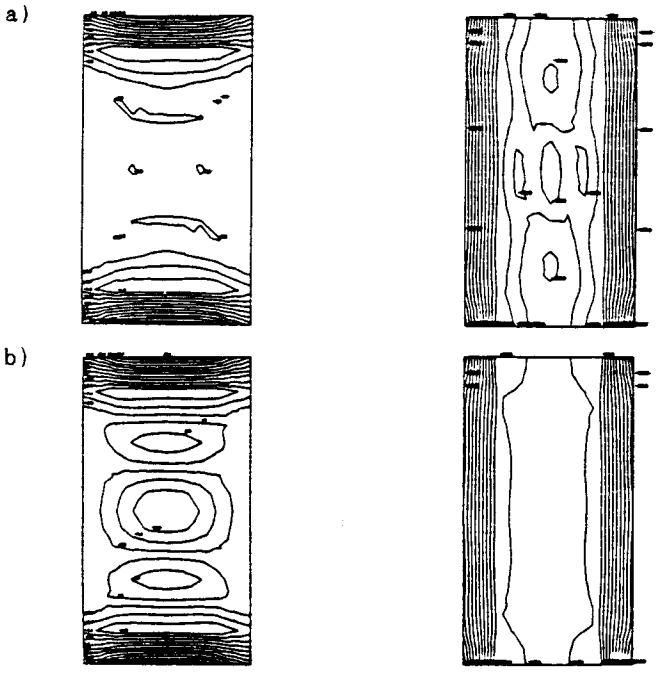

Fig. 11 Isolines of the horizontal and vertical stresses (sliding boundaries)

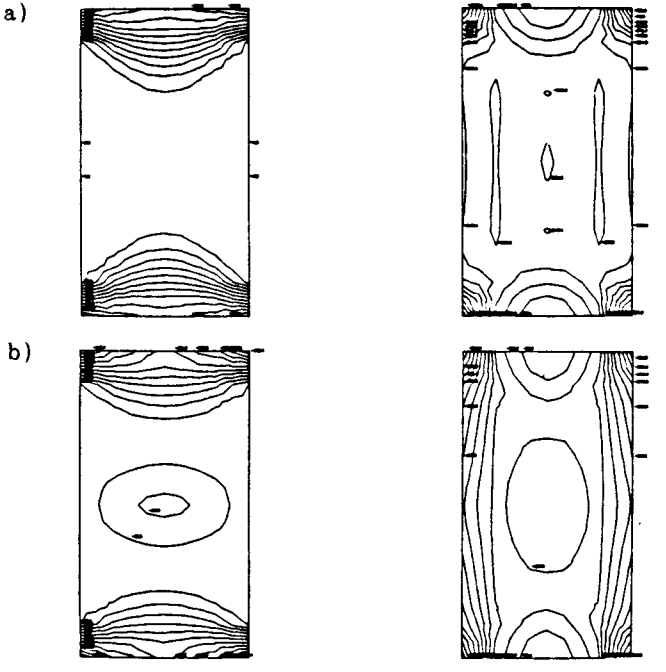

Fig. 12 Isolines of the horizontal and vertical stresses (fixed boundaries)

crack front reaches roughly to the upper and lower quarter of the specimen length. Subsequently, during post-peak softening (Fig. 10d), the crack front propagate further towards the loading platens, which is also evident from Fig. 11a and 11b, in which the isolines of the horizontal and vertical normal stresses at the peak load state and in the final post-peak softening state are plotted.

In the case of fixed boundaries, the mechanism of failure is similar (Fig. 10 and 12). The crack starts to propagate from the weak zone at the center of the specimen and moves first towards the loading platens. Then, however, already before reaching the peak-load state, the crack propagations changes to two inclined directions; this happens while the crack reaches roughly to the top and bottom quarters of the specimen height.

Numerical results reveal that horizontal tensile stresses at the crack front are greater for the case of sliding boundaries, while the compressive normal stresses after the crack closing at the center of the specimen are greater for the specimen with fixed boundaries. For both cases, calculations indicate a very large volume dilatancy at the center of the specimen.

To investigate the size effect, the aforementioned calculations have been run for geometrically similar specimens of three different sizes of the ratio 1:2:4, the smallest specimen having the height $h = 6l = 540$ mm. It is highly interesting, although perhaps not surprising with respect to the knowledge from experiments, that no significant size effect has been detected from the calculated results.

This means that compression fracture is not driven by the stored elastic energy that is released globally from the entire specimen. Rather, it must be driven by a local mechanism near the fracture front, which is approximately independent of the specimen shape and boundaries, and thus involves no significant stress changes farther away from the crack band front.

It is also interesting that if a slight nonsymmetry is introduced into the computational model (e.g., slightly nonsymmetric nodal coordinates), the force displacement curve as well as the failure mode for these specimens remain the same.

It should be also noted that asymmetry is introduced into the specimen model if the directions of the rectangular components of the shear stress vector on the microplane are not introduced systematically the same for all the integration points. Rather, these directions have bee assigned randomly. The role of this nonsymmetry becomes stronger if the initial shear moduli are larger. Thus, using by assigned shear component directions, the failure mode is always nonsymmetric (and of shear band type), even in the case of geometrically symmetric specimens. In this regard it needs to be pointed out that, in contrast to the calculations in the first two examples of the present paper, the microplane model for the splitting fracture examples involved shear microplane strain vectors that were split into two mutually orthogonal components. As a consequence, hypothesis II is not valid in this version of microplane model, i.e., the shear strain and stress vectors within each microplane are not parallel.

It may also be noted from the Fig. 9 and 10 that the tendency to the development of shear bands exists at the beginning in the specimen with sliding boundaries, but is later overridden by axial propagation. In the specimen with fixed boundaries, on the other hand, there is a tendency to shear band formation near the specimen corners in final stage.

The compression failure was previously investigated by a very different nonlocal constitutive model, namely a nonlocal version of the Drucker-Prager plasticity model with a degrading yield limit (Bažant and Droz, 1988). In that study it was found that the response path of a perfectly symmetric specimen bifurcates, after which either two crossing shear bands may grow or only one may grow while another one unloads. The condition of path stability also indicated that only the asymmetric propagation of a one inclined shear band is the correct solution even if there is perfect symmetry in the specimen. Path stability checks based on the tangential stiffness matrix are not included in the present study, however due to the lack of symmetry there should have been no bifurcations. Thus it seems that the symmetric crossing shear bands in Fig. 11 are the correct solution, and the reason that this is so is probably due to the fact that they exist only for a short stage of the response, being later overpowerd by axial crack propagation.

CONCLUSION

The nonlocal generalization of the microplane model with normal microplane strains that are split into volumetric and deviatoric components is a powerfull and very general material model for concrete. It is capable of describing not only nonlinear triaxial test results for compressive and shear stress states, including post-peak softening, but also tensile fracture as well as fracture in compression (both shear bands and axial splitting). The nonlocal generalization is of the nonlocal damage type, in which only the variables that control strain softening are calculated from spatial averages of the macrostrain tensor, while all the remaining variables, especially the elastic strains, are local.

Acknowledgments. - Support under AFOSR contract No. F49620-87-C-0050DEF is greatfully acknowledged. Partial support for fracture studies was also received from the Center for Advanced Cement-Based Materials at Northwestern University (NSF grant DMR-8808432). Furthermore, part of the work of the first author was done at the Lehrstuhl für Mechanik, Technical University of Munich, under support through Humboldt Award of Senior U.S.Scientist. Thanks are also due to T. Hasegawa, a Visiting Scholar at Northwestern University on leave from Shimizu Construction Co., Tokyo, for some valuable discussions.

REFERENCES

1. Bažant, Z.P., "Numerically stable algorithm with increasing time steps for integral-type aging creep", Proc., First Int. Conf. on Struct. Mech. in Reactor Technology, West Berlin, T.A. Jaeger, ed., Vol. 4, Part H, 1971, pp. 119-126.

2. Bažant, Z.P., and Gambarova, P.G., Crack shear in concrete: crack band microplane model. J. Struc. Eng., ASCE,110(9), pp. 2015-2035, 1984.

3. Bažant, Z.P., Microplane model for strain-controlled inelastic behaviour, Mechanics of Engineering Materials, C.S. Desai and R.H. Gallager, eds., John Wiley & Sons, Chichester and New York, chap. 4, 1984, pp. 45-59.

4. Bažant, Z.P., Imbricate continuum and its variational derivation. J. of Eng. Mech., ASCE, 110(12), pp. 1693-1712, 1984.

5. Bažant, Z.P., Belytschko, T.B., and Chang, T.P., Continuum model for strain softening. ASCE J. of Eng. Mech. 110 (12), pp. 1666-1692, 1984.

6. Bažant, Z.P., and Oh, B.-H., Microplane model for progressive fracture of concrete and rock. J. of Eng. Mech., ASCE, 111(4), pp. 559-582, 1985.

7. Bažant, Z.P., and Chern, J.-C., Strain softening with creep and exponential algorithm. J. of Eng. Mech., ASCE, 111(3), pp. 381-390, 1985.

8. Bažant, Z.P., and Oh, B.-H., Efficient numerical integration on the surface of a sphere. Zeitschrift für angewandte Mathematik und Mechanik ZAMM, 66(1), pp. 37-49, 1986.

9. Bažant, Z.P., and Pfeiffer, P.A., Determination of fracture energy from size effect and brittelness number." ACI Materials Journal, 84, pp. 463-480, 1987.

10. Bažant, Z.P., and Prat, P.C., Microplane model for brittle-plastic material - parts I and II. J. of Eng. Mech., ASCE, 114(10), pp. 1672-1702, 1988.

11. Bažant, Z.P., and Pijaudier-Cabot, G., Nonlocal continuum damage, localization instability and convergence. J. of Appl. Mech., ASME, 55, pp. 287-293, 1988.

12. Bažant, Z.P., and Ozbolt, J., Nonlocal microplane model for fracture, damage and size effect in structures, Report 89-10/498n Center for Concrete and Geomaterials, Northwestern University, Evanston, 1989, 33 pp..

13. Bažant, Z.P., Tabbara M.R., Kazemi, M.T., and Pijaudier-Cabot G., Random particle model for fracture of aggregate or fiber composits, Report 89-7/498r Center for Advanced Cement-Based Materials, Northwestern University, Evanston, 1989, pp. 24.

14. Bazant, Z.P., and Cedolin, L., Stability of structures: elastic, inelastic, fracture and damage theories and codes, Oxford University Press, New York, 1990 (in press).

15. Droz, P., and Bazant, Z.P., Nonlocal Analysis of Stable States and Stable Paths of Propagation of Damage Shear Bands, Strain Localization and Size Effect due to Cracking and Damage, J. Mazars and Z.P. Bazant, eds., Elsevier Appl. Sci., London and New York, 1986, pp. 415-425.

16. Eringen, A.C., and Edelen, D.G.D., On nonlocal elasticity. Int. J. of Eng. Sci. 10, pp 233-248, 1972.

17. Kröner, E., Interrelations between various branches of continuum mechanics. Mech. of Generalized Continuua, E. Kröner, ed., Springer, W.Berlin, pp. 330-340, 1968.

18. Krumhansl, J.A., Some considerations of the relations between solid state physics and generalysed continuum mechanics. Mech. of Generalized Continuum, E. Kröner, Ed., Springer, W.Berlin, pp. 298-331, 1968.

19. Levin, V.M., The relation between mathematical expectation of stress and strain tensor in elastic micro-heterogenous media. Prikl. Mat. Mehk. 35, pp. 694-701, 1971 (in Russian).

20. Pijaudier-Cabot, G., and Bazant, Z.P., Nonlocal damage theory. J. of Eng. Mech., ASCE, 113, pp.1512-1533, 1987.

21. Roelfstra P.E., and Wittmann, F.H., Numerical modelling of fracture of concrete, SMiRT 9 (Lausanne), Transactions, Balkema, Rotterdam, Vol. H., 1987, pp. 41-49.

22. Stroud, A.H., Approximate calculation of multiple integrals, Prentice Hall, Englewood Cliffs, N.J., 1971.

23. Taylor, G.I., Plastic strain in metals. J. of Inst. of Metals, Vol. 62, pp. 307-324, 1938.

24. Pande, G.H., and Xiong, W., An improved multi-laminate model of jointed rock masses, First Int. Symposium on Numerical Models in Geomechanics, 1982, pp. 218-226.

25. Zienkiewicz, O.C., and Pande, G.N., Time-dependent multi-laminate model of rocks -- a numerical study of deformation and failure of rock masses. Int. Jour. of Num. and Anal. Meth. in Geomechanics, 1, pp. 219-247, 1977.

26. Zubelewicz, A., and Bažant Z.P., Interface element modelling of fracture in aggregate composites. J. of Eng. Mech. Div., ASCE, 113 (11), pp. 1619-1630, 1987.